9.4 A MODIS-BASED CONTRAIL CLIMATOLOGY OF COVERAGE AND CLOUD PROPERTIES

David P. Duda*, Rabi Palikonda, Konstantin Khlopenkov, Sarah Bedka, Thad Chee
Science Systems and Applications, Inc., Hampton, Virginia

Patrick Minnis
NASA Langley Research Center, Hampton, Virginia

1. INTRODUCTION

Accurate measurements of contrail coverage are essential for accurate estimates of global contrail radiative forcing. Nearly all estimates of global radiative forcing from line-shaped contrails use estimates of regional contrail coverage derived from satellite imagery. Although several studies of regional contrail coverage are available, no comprehensive study of the coverage of both the conterminous United States (CONUS) and Europe using the same satellite dataset has been produced. Estimates of contrail coverage over both regions from current numerical models show considerable uncertainty, and research programs including the Aviation-Climate Change Research Initiative (ACCRI) have recognized the need to develop a global climatology of line-shaped contrails from a homogeneous set of satellite data to reduce this model uncertainty.

We use an automated contrail detection algorithm (CDA) to determine the coverage of line-shaped persistent contrails over the CONUS and European regions. The contrail detection algorithm is a modification of the Mannstein et al. (1999) method, and uses several channels from the *Terra* and *Aqua* MODerate-resolution Imaging Spectroradiometers (MODIS) to reduce the occurrence of false positive detections. In addition, we compute the visible optical depth and longwave radiative forcing to several months of MODIS data over the two aviation-intense regions to provide a more homogeneous, accurate, and statistically significant dataset for model validation and analysis of contrails.

2. CONTRAIL DETECTION ALGORITHM

The contrail detection algorithm (CDA) (Duda et al., 2010) is a modified version of the technique described by Mannstein et al. (1999), which detects linear contrails in multi-spectral thermal infrared (IR) satellite imagery using only two channels (11 & 12 μm) from the Advanced Very High Resolution Radiometer (AVHRR). This method requires only the brightness temperatures BT) from the two channels, with no other supporting data, and can be applied to both day and night scenes. It uses a scene-invariant threshold to detect cloud edges produced by contrails, and 3 binary masks to determine if the detected linear features are truly contrails. However, these masks are not always sufficient to remove all non-edge features. To reduce the number of false positive detections due to lower cloud streets and surface features, we add observations from other IR radiance channels available on the MODerate-resolution Imaging Spectroradiometer (MODIS) on *Terra* and *Aqua*. The new modified method uses additional masks derived from the added thermal infrared channels to screen out linear cloud features that appear as contrails in the original method.

The modified CDA follows the same overall data flow as the original Mannstein et al. CDA. The IR brightness temperature measurements are first normalized to allow the data to be compared with scene-invariant thresholds. In addition to the T12.0 (inverted BT for the 12.0 μm measurements) and BTD1 (BT difference between the 10.8 and 12.0 μm measurements) used in the original CDA, the modified CDA also uses the following BT data:

T6.8 – water vapor channel (6.8 μm) BT
BTD2 = (T8.6 – T12.0),
BTD3 = (T8.6 – T13.3),
BTD4 = (BTD1 + BTD2).

The sum of the normalized images N=N12.0 + NBTD1 + NBTD2 was then convolved with a line filter of 19×19 pixels in 16 different directions, and the individual connected regions resulting from the filtering are considered as possible contrail objects. These objects are then checked against 6 binary masks to check for contrails. The first three masks are similar to the original CDA:

A. N = NBTD4 + NBTD2 + N6.8 + N12.0
+ NBTD1 > 3.45 K.
B. BTD1 > 0.2 K.
C. Gradient(12.0 μm) < 2×STD(12.0 μm) + 1 K.

The threshold in condition A selects pixels having a higher-than-average normalized brightness, which is typical of thin cirrus in the BT difference (BTD) imagery. The relatively low BTD1 threshold was retained from the original CDA to allow detection of possible contrails over lower opaque clouds. Condition C compares the large-

*Corresponding author address: David P. Duda, Science Systems and Applications, Inc., 1 Enterprise Parkway, Hampton, VA 23666; e-mail: david.p.duda@nasa.gov.

scale maximum gradient for 12.0 μm in a 15×15 pixel vicinity of a possible contrail pixel with the local standard deviation to eliminate features like coastlines which also appear as lines in the normalized 12.0 μm images.

Three additional binary masks are included in the modified CDA:

D. (Gr(6.8) – Gr(12.0)/(Gr(12.0) + 0.03) > -0.85.
E. NBTD3 > 0.0 K.
F. Gradient(BTD3) < 1.5×STD(BTD3) + 0.2 K.

All three masks are used to reduce the number of false positive detections of lower level cloud streets and other edge features in the IR imagery. Condition D compares the large-scale maximum gradient for the 6.8-μm water vapor channel with the gradient from the 12.0-μm channel. The water vapor channel tends to be smooth except in regions with high clouds, while the 12.0-μm channel shows cloudiness at all levels in the atmosphere. Thus, condition D removes regions where only low clouds are likely in the imagery. Condition E tends to mask regions with lower clouds more than areas with higher clouds, while condition F is similar in function to condition C.

As part of the quality control in the contrail detection algorithm, a two-step process removes striping in the MODIS thermal infrared imagery. The MODIS instrument consists of an array of independent scanning sensors that may induce striping in raw images that is especially apparent in BTD imagery. In the first step, data from failing detectors in the MODIS instrument are replaced by data interpolated from measurements with neighboring lines. Next, the image is processed with an FFT filter as overlapping blocks of pixels. For each block, the Fourier frequency spectrum is corrected to suppress frequencies that are multiples of 10 (the number of independent sensors in MODIS). The restored image has almost no striping noise but preserves the contrails seen in the BTD imagery.

To provide a standard geographic grid for the contrail data, all of the MODIS imagery is then re-gridded to a Lambert Azimuthal Equal-Area projection. The re-projected data have reduced effects of image distortion at large (> 50 degrees) viewing angles (including MODIS "bow-tie" effects), and thus extend the usable area of contrail detection to the entire MODIS image. Earlier studies including Mannstein et al. (1999) used the original unmodified satellite projection, and thus analysis had to be limited to viewing angles less than 50 degrees to avoid over-detection of elongated clouds as contrails at the edges of the imagery.

3. CDA DEVELOPMENT

By varying the thresholds in the binary masks used in the modified CDA, it is possible to develop conservative masks that produce few false alarms or more sensitive masks that have a high level of false alarms but also detect more contrails. Six sets of thresholds were established with CDA0 as the most conservative mask and CDA5 as the most sensitive contrail mask. The most sensitive mask (CDA5) also included two (instead of one) additional re-sampling steps (Mannstein et al., 1999) that allow the detection of wider contrails. The choice of CDA sensitivity is not only important for contrail coverage estimation, but also for the retrieved contrail properties. Preliminary results show that the most sensitive CDA detects more contrails, and the contrail optical depth (COD) range increases, with increases in the relative number of both very thin (COD < 0.05) and thick (COD > 0.6) contrails.

To develop a climatological database of contrail coverage and optical properties, it is necessary to determine which CDA is best. It is assumed here that the optimal CDA is the one that produces the smallest bias, while minimizing the false alarm rate. Thus, the optimal method will produce roughly the same amount of false contrail and missed contrail pixels. To determine this optimal technique, a subjective error analysis was performed using an updated version of the interactive program developed by Minnis et al. (2005). The CDAs were first applied to sets of 22 daytime and 20 nighttime MODIS images covering the four mid-season months (January, April, July, and October) over CONUS. Four different analysts evaluated the images interactively to estimate the number of false detections, missed contrails, and positive contrail detections. A composite mask for each pixel of the image was determined from the majority result of the four analysts. The results from CDAs 0-5 were then evaluated with this composite mask. Overall, it was found that CDA2 and CDA3 produced the smallest biases (relative biases closest to unity) for night and day, respectively (See Figure 1.)

While it is assumed that the analysts' subjective assessments constitute the "truth" set for the CDA selection, it is apparent in viewing many of the MODIS images that defining a linear contrail is not always straightforward. This difficulty arises primarily from the presence of older contrails that have spread significantly. Close inspection of the imagery suggests some clouds in the imagery are very likely older contrails that have lost some of their distinct contrail "signatures", having diffused, overlapped, and grown in particle size. This evolution is common (Minnis et al., 1998), especially in contrail outbreaks (Carleton et al., 2008). Such outbreaks may be responsible for much of the excess cloudiness due to contrails, but are difficult to quantify with automated methods. The ambiguity resulting from the older and overlapping contrails in such outbreaks should be considered when defining the extent of linear contrails. Since the spreading contrails do not appear to be included in the current reference dataset, it is likely that the truth set from the analysts is

an underestimate and the corresponding CDA results will also underestimate the true contrail coverage.

4. CONTRAIL COVERAGE ESTIMATES

The CONUS and Europe are two areas with the some of the heaviest air traffic over the globe, and most contrail observation and modeling efforts have focused on determining contrail coverage in these regions. This study is the first to show observed coverage estimates from both regions using the same measurement framework. Figure 2 shows the combined day and nighttime contrail coverage detected with the CDA from *Terra* MODIS data using the optimal thresholds determined by the visual analysis (CDA3 for day and CDA2 for night) for the mid-seasonal months (January, April, July and October (JAJO)) of 2006. The mean contrail coverage determined over the CONUS for the 4 months is 0.15 percent, which is a factor of 4 times smaller than the coverage determined by Palikonda et al. (2005) from AVHRR data. Figure 3 shows the combined day and nighttime contrail coverage determined by CDA3 over Europe from *Terra* MODIS data for JAJO 2006. The 4-month mean contrail coverage over Europe is nearly the same as over CONUS (0.17 percent). Over both the CONUS and Europe, the greatest and least contrail coverage occur during winter and summer, respectively, in response to seasonal changes in upper tropospheric temperature and humidity. Both Figures 2 and 3 show that detected contrail coverage appears to be suppressed over mountainous regions (Rockies in CONUS and Alps in Europe). This feature has been noted in earlier studies including Mannstein et al., and is caused by the thermal heterogeneity of the background, which increases with elevation and terrain height variability. Methods to correct for the thermal heterogeneity effects have been developed by Mannstein et al. (1999) and Meyer et al. (2002). Figure 4 shows how applying the three-step method described by Meyer et al. (2002) to the Terra CONUS results increases the overall coverage 60 percent.

A comparison of the current results over central Europe with the annual mean uncorrected data from the Mannstein et al (1999) study [not shown] showed similar coverage patterns and an identical mean contrail coverage of 0.23 percent, although the Mannstein et al study used AVHRR data from 1996 while the current study used MODIS data from 2006. These results show that the new CDA finds fewer contrails than found with the earlier Mannstein et al. method. It is likely that the CDA misses many of the thicker, wider contrails observed in the imagery. However, while it is clear that many contrails, especially thicker ones, are missed using the CDAs developed here, the number of clouds mistaken as contrails has been reduced significantly relative to previous studies.

5. CORRECTIONS TO CONTRAIL COVERAGE

As mentioned above, it is apparent that in meteorological conditions favorable for contrail outbreaks, estimates of linear contrail coverage from the automated method described here may be less than the true contrail coverage. To obtain an estimate of how frequently such contrail outbreaks may occur, the contrail coverage from the CONUS results are plotted in Figure 5. For both *Aqua* and *Terra* imagery, the distribution of contrail amount detected in each 5-minute granule has a similar distribution, with more contrail outbreaks (defined here as images with more than 16,000 detected contrail pixels per granule) during the daytime than at night. For the daytime, approximately 4 percent of the images have contrail outbreaks, which make up 16 percent of the detected coverage. At night, only 1 percent of the images are classified as having contrail outbreaks, comprising 5.5 percent of the total detected nighttime contrail pixels. Contrail outbreaks make up a significant portion of the contrail coverage, and thus the underestimation of contrail coverage in outbreaks must be addressed.

To overcome some of the difficulties in estimating contrail coverage within a widespread outbreak, some methods are being developed to detect at least some of the more diffuse contrail-related cloudiness. One approach is to loosen the thresholds applied in the CDA in MODIS images where large amounts of contrail coverage are expected. An example of this method is shown in Figure 6. Figure 6a shows the BTD1 image from *Aqua* MODIS taken at 1840 UTC 1 Jan 2006. A large contrail outbreak east of FL produced several contrails (and more diffuse contrail cirrus) that are visible in the image, especially in the upper right quarter of the picture. Figure 6b shows the contrail pixels detected using the CDA3 threshold. Many of the thicker contrails are missed by this version of the CDA. By adjusting the thresholds in the CDA (Figure 6c) more contrail coverage can be detected. Care would be necessary to apply the more sensitive CDA only in images where the increase in contrail detections offsets the increase in the number of false positive detections in the imagery. Some false detections are apparent in Figure 6c on the left hand side of the image.

Another way to increase the number of contrail detections would be to expand the allowable width of the detected contrails in the retrieval. This can be done to some extent by determining a set of radiances characteristic of the more certain detected contrails and performing a search of the contrail surrounding for pixels having similar radiances. An example of this technique is shown in Figure 6d using the CDA3 mask as the starting point for this widening algorithm. As with the previous approach, this method will also lead to some false positive detections, and the limitation of these methods will depend on the false alarm rate that is generated by each approach.

Other improvements are planned that will be included with the final contrail detection algorithm. In addition to the background heterogeneity correction mentioned above, information from the ACCRI flight waypoint dataset provided by the US DOT Volpe Center and upper tropospheric humidity and wind data from the Modern Era Retrospective-analysis for Research and Applications (MERRA) analyses (Reincker et al., 2011) can be useful in determining a more accurate measure of contrail coverage. For example, a combination of the ACCRI flight track database and the MERRA analyses can be used to simulate the orientation and proximity of contrails (along with estimates of error in the wind, humidity and aircraft location data) that can be compared with contrails detected by the CDA to remove false positives, especially in areas where flight densities are low. This method would be especially helpful in the tropics where thin cirrus streamers from convective outflow and subtropical jet streams are often mistaken by the CDA as contrails. Efforts to use the flight track data are underway to assign a detection confidence value to the contrail pixels retrieved by the CDA, but more work is needed to refine this method.

6. CONTRAIL OPTICAL PROPERTIES

After detecting the contrails, the COD and the longwave radiative forcing of the contrails are determined using the same techniques employed by Palikonda et al. (2005), except that the contrail temperature is assumed to be 220 K instead of 224 K. Examples of the COD distributions averaged over the four mid-season months from 2006 for the CONUS and Europe are shown in Figure 7. The mean COD over the CONUS (0.200) is slightly larger than the mean COD computed over Europe (0.176). This difference in COD between CONUS and Europe is smaller than the difference in COD computed in previous studies. Palikonda et al. (2005) calculated a mean COD of 0.26 over the CONUS, while Meyer et al. (2002) computed a mean COD of 0.11 over Europe. Figure 8 shows the distribution of mean longwave contrail radiative forcing (LWCRF) for both regions computed for JAJO 2006. The mean LWCRF over CONUS (11.2 W m^{-2}) is 24 percent larger than the mean LWCRF computed over Europe (9.0 W m^{-2}).

7. FUTURE WORK

The contrail coverage presented here will be part of a Northern Hemisphere contrail climatology that is under development. The contrail climatology will provide a more consistent empirical estimate of contrail radiative forcing and cloud properties that can be used for the improvement and validation of contrail models. In addition to the work on improving contrail detection, we also will continue to refine cloud property retrieval algorithms so that contrail and cloud properties for the entire Northern Hemisphere will be retrieved from one or two years of *Terra* and *Aqua* MODIS data. We are also developing improved radiative forcing estimation methods using the NASA LaRC CERES cloud product retrieval system (Minnis et al., 2008, 2011). All of the contrail coverage and property results will be made available to modelers in accessible formats such as netCDF.

8. REFERENCES

Carleton, A., Travis, D. J., Master, K., and Vezhapparambu, S., 2008: Composite atmospheric environments of jet contrail outbreaks for the United States," *J. Appl. Meteorol Climatol.*, 47, 641-667.

Duda, D. P., K. Khlopenkov, and P. Minnis, 2010: Two new contrail detection methods for the compilation of a global climatology of contrail occurrence. *Extended Abstracts, 13th Conf. on Cloud Physics,* Portland, OR, Amer. Meteor. Soc., P2.76. [Available online at http://ams.confex.com/ams/pdfpapers/171549.pdf.]

Mannstein, H, R. Meyer, P. Wendling, 1999: Operational detection of contrails from NOAA-AVHRR data. *Int. J. Remote Sensing,* 20, 1641-1660.

Meyer. R., H. Mannstein, R. Meekötter, U. Schumann, and P. Wendling, 2002: Regional radiative forcing by line-shaped contrails derived from satellite data. *J. Geophys. Res*. 107, doi:10.1029/2001JD000426.

Minnis, P., Young, D. F., Nguyen, L., Garber, D. P., Smith, W. L., Jr., and Palikonda, R., 1998: Transformation of contrails into cirrus during SUCCESS, *Geophys. Res. Lett.*, 25, 1157-1160.

Minnis, P., Palikonda, R., Walter, B. J., Ayers, J. K., and Mannstein, H., 2005: Contrail properties over the eastern North Pacific from AVHRR data, *Meteorol. Z.,* 14, 515-523.

Minnis, P., and Co-authors, 2008: Cloud detection in non-polar regions for CERES using TRMM VIRS and Terra and Aqua MODIS data. *IEEE Trans. Geosci. Remote Sens.*, 46, 3857-3884.

Minnis, P., and Co-authors, 2011: CERES Edition-2 cloud property retrievals using TRMM VIRS and Terra and Aqua MODIS data. *IEEE Trans. Geosci. Remote Sens.*, 49, doi:10.1029/TGRS2011.2144601.

Palikonda, R., Minnis, P., Duda, D. P., and Mannstein, H., 2005: Contrail coverage derived from 2001 AVHRR data over the continental United States of America and surrounding areas, *Meteorol. Z.,* 14, 525-536.

Riencker, M. M. et al., 2001: MERRA – NASA's Modern-Era Retrospective Analysis for Research and Application, *J. Climate*, doi: 10:1175/JCLI-D-11-000015.1, in press.

Acknowledgements. This research is supported by the FAA ACCRI program, and by funding from the American Recovery and Reinvestment Act (ARRA).

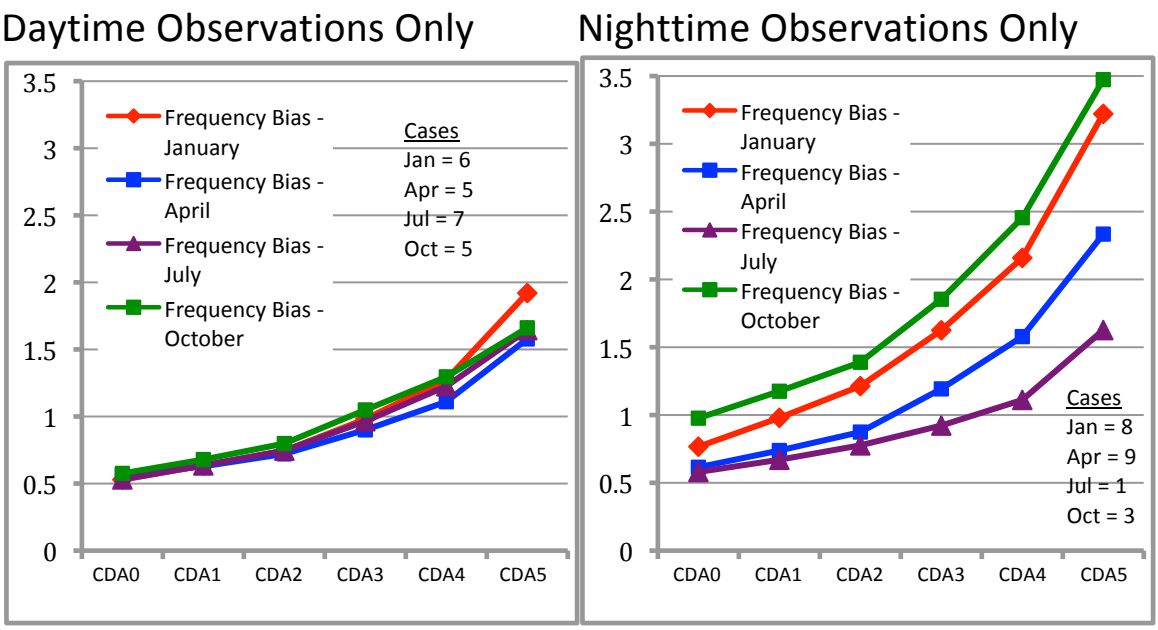

Figure 1: Frequency bias for six test case contrail detection algorithms (CDAs). The sensitivity of the CDA thresholds increases from left to right.

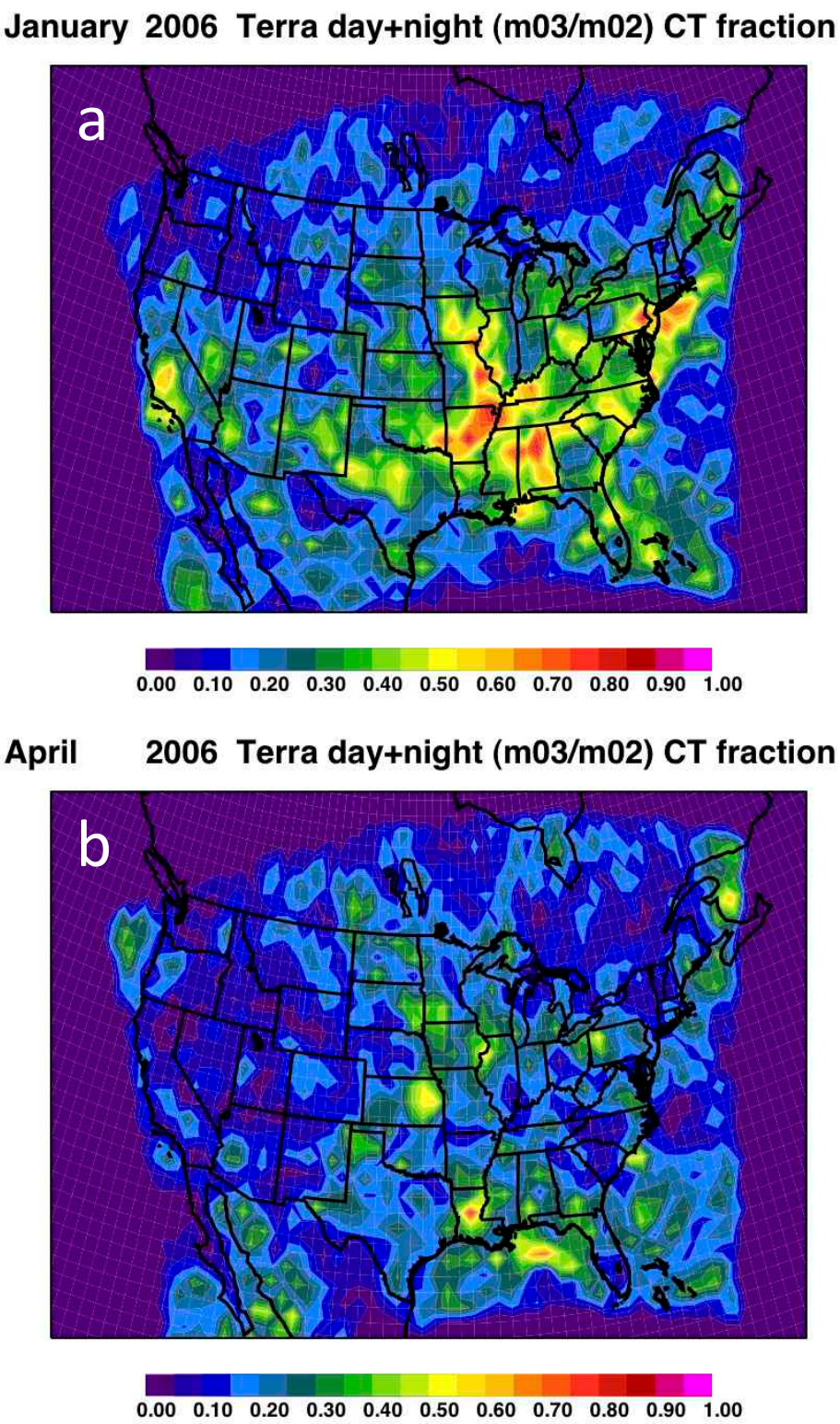

Figure 2: (a) Monthly mean uncorrected day (from CDA3) + night (from CDA2) contrail coverage over CONUS from Terra MODIS measurements during January 2006. The contrail coverage is expressed in percent. (b) Same as (a), but for April 2006. (c) Same as (a), but for July 2006. (d) Same as(a), but for October 2006.

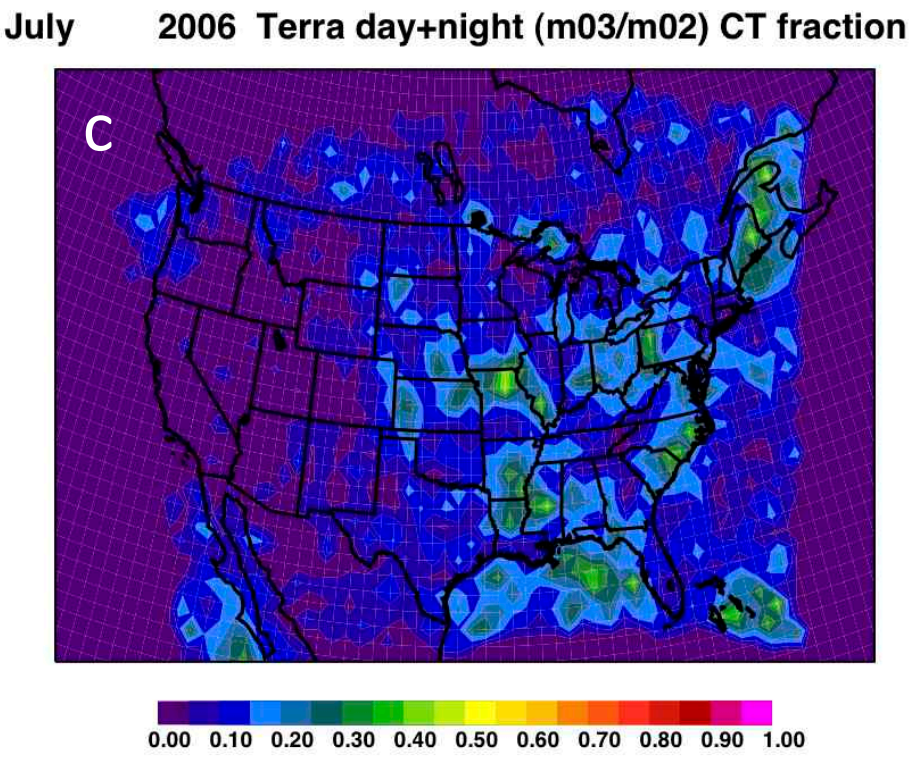

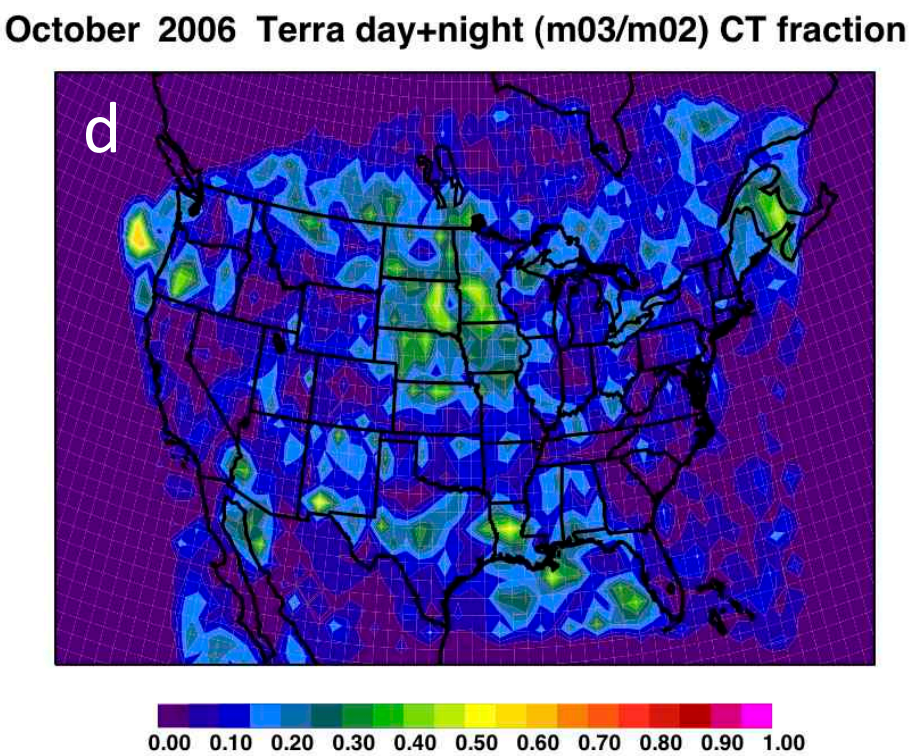

Figure 2 (continued): (a) Monthly mean uncorrected day (from CDA3) + night (from CDA2) contrail coverage over CONUS from Terra MODIS measurements during January 2006. The contrail coverage is expressed in percent. (b) Same as (a), but for April 2006. (c) Same as (a), but for July 2006. (d) Same as(a), but for October 2006.

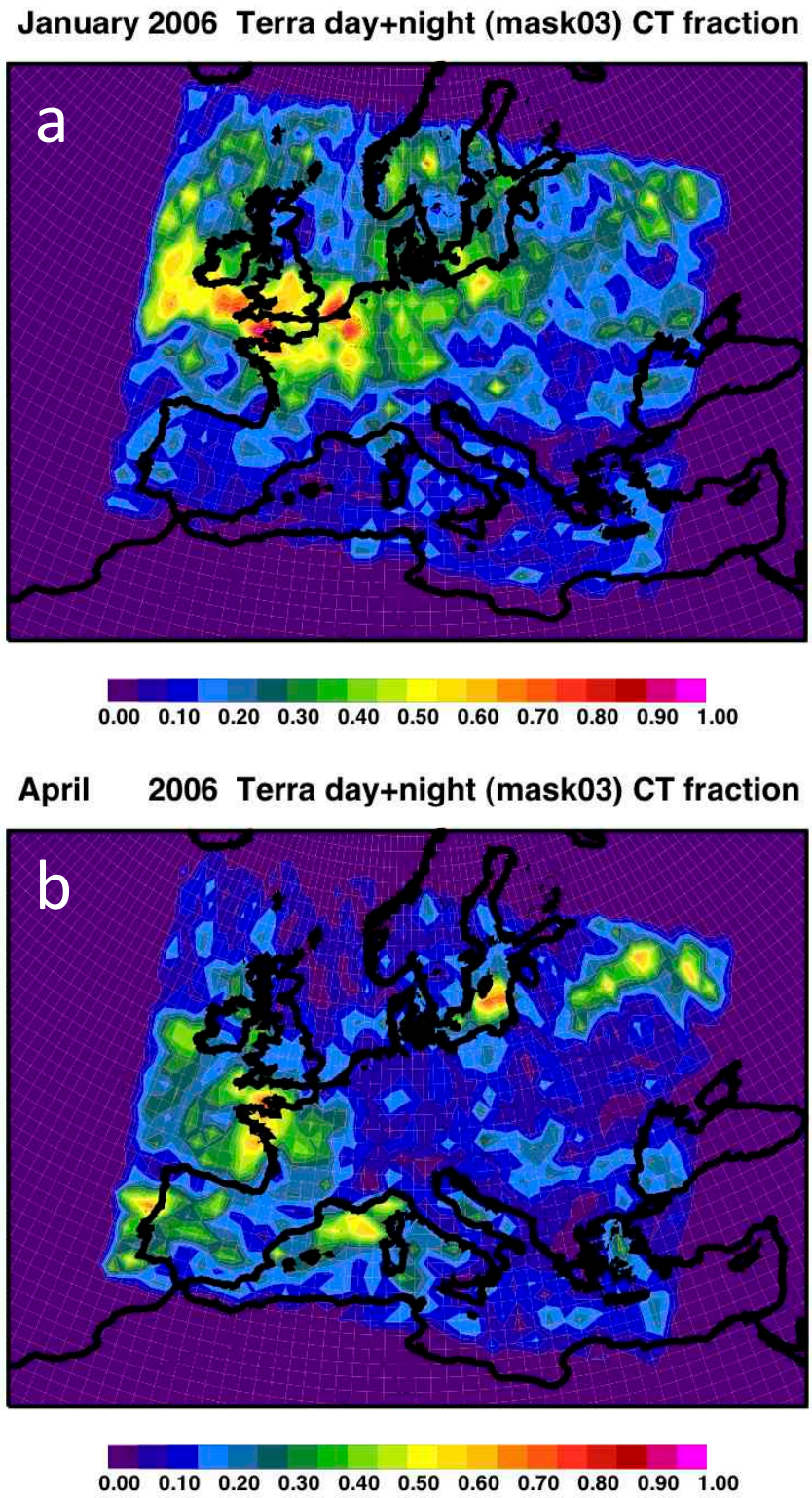

Figure 3: (a) Monthly mean uncorrected day + night contrail coverage derived by CDA3 over Europe from Terra MODIS measurements during January 2006. The contrail coverage is expressed in percent. (b) Same as (a), but for April 2006. (c) Same as (a), but for July 2006. (d) Same as(a), but for October 2006.

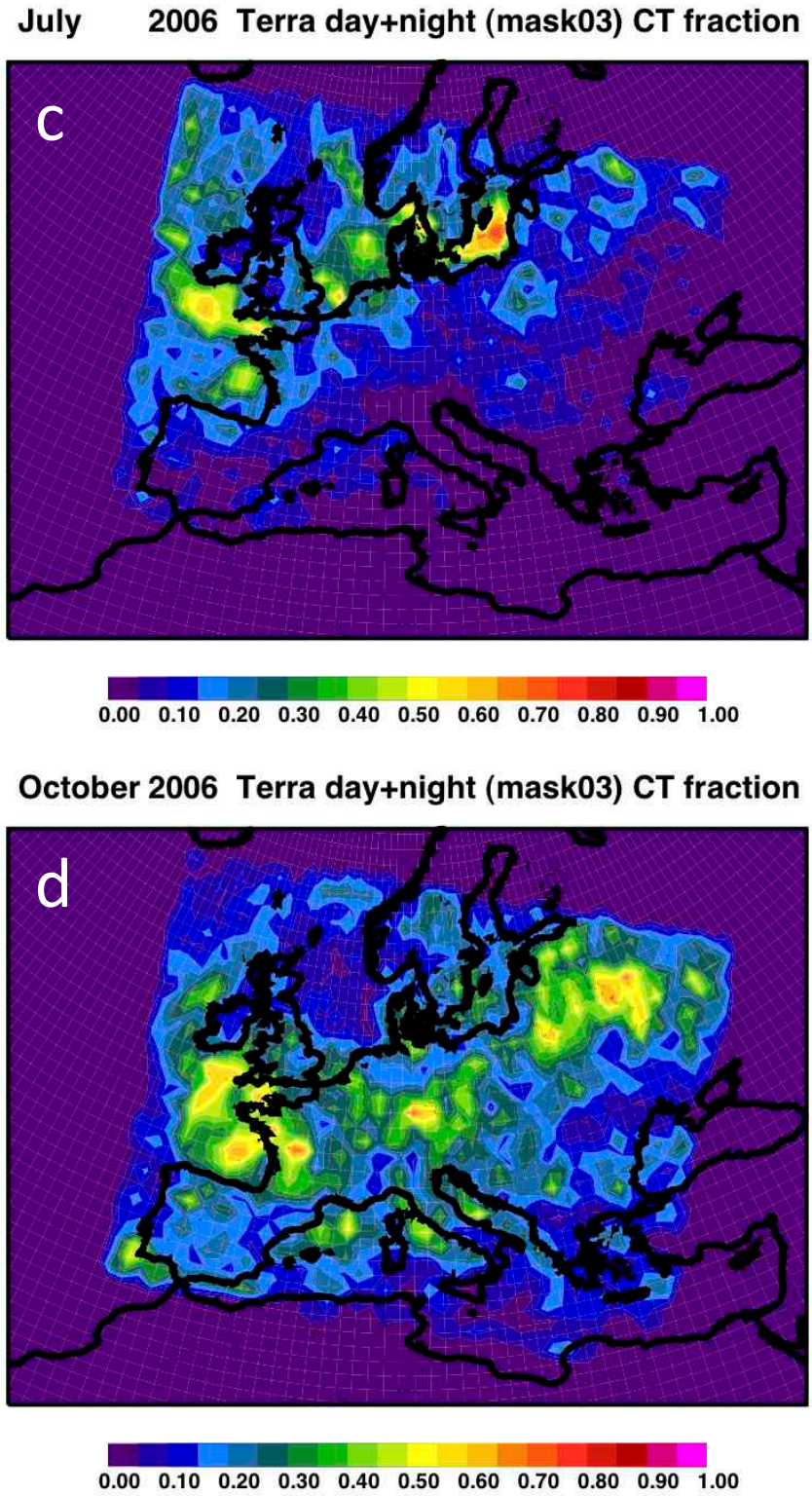

Figure 3 (continued): (a) Monthly mean uncorrected day + night contrail coverage derived by CDA3 over Europe from Terra MODIS measurements during January 2006. The contrail coverage is expressed in percent. (b) Same as (a), but for April 2006. (c) Same as (a), but for July 2006. (d) Same as(a), but for October 2006.

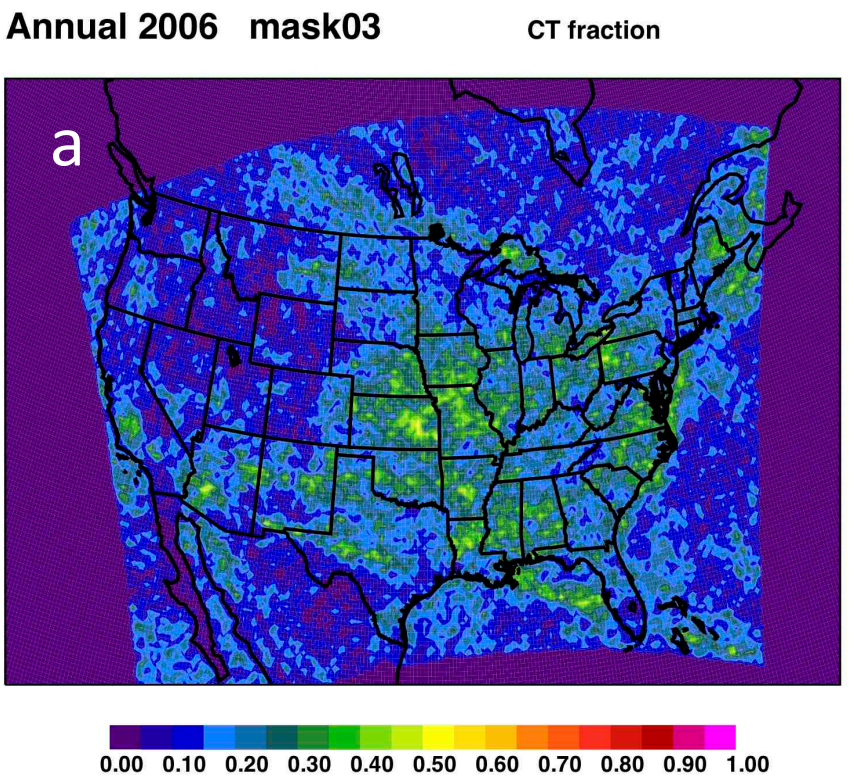

Figure 4: (a) Annual mean uncorrected day + night contrail coverage (in percent) derived by CDA3 over CONUS from Terra MODIS. (b) Annual mean contrail coverage from (a) corrected by method following Meyer et al. (2002).

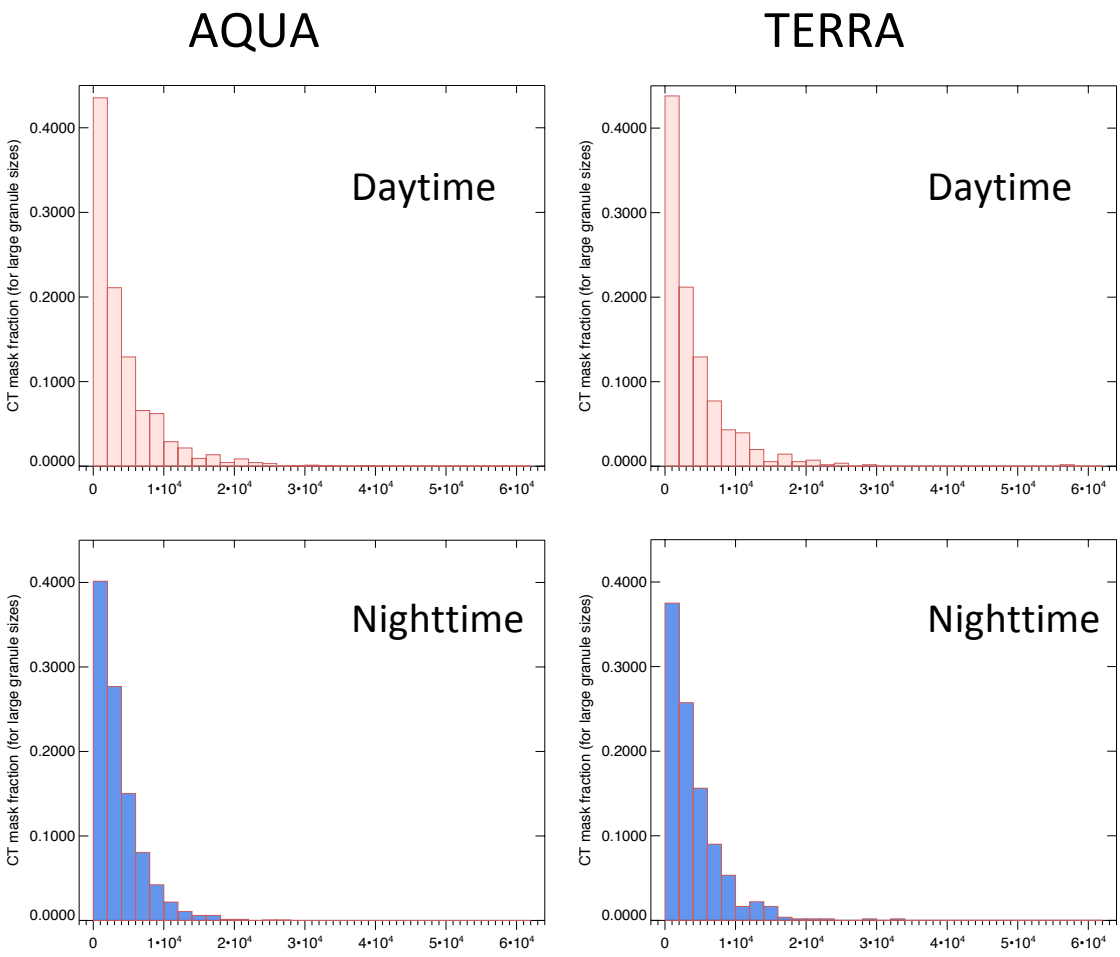

Figure 5: Normalized histograms of detected contrail amount for MODIS granules located over the CONUS for 2006. Frequency bias for six test case contrail detection algorithms (CDAs). The sensitivity of the CDA thresholds increases from left to right.

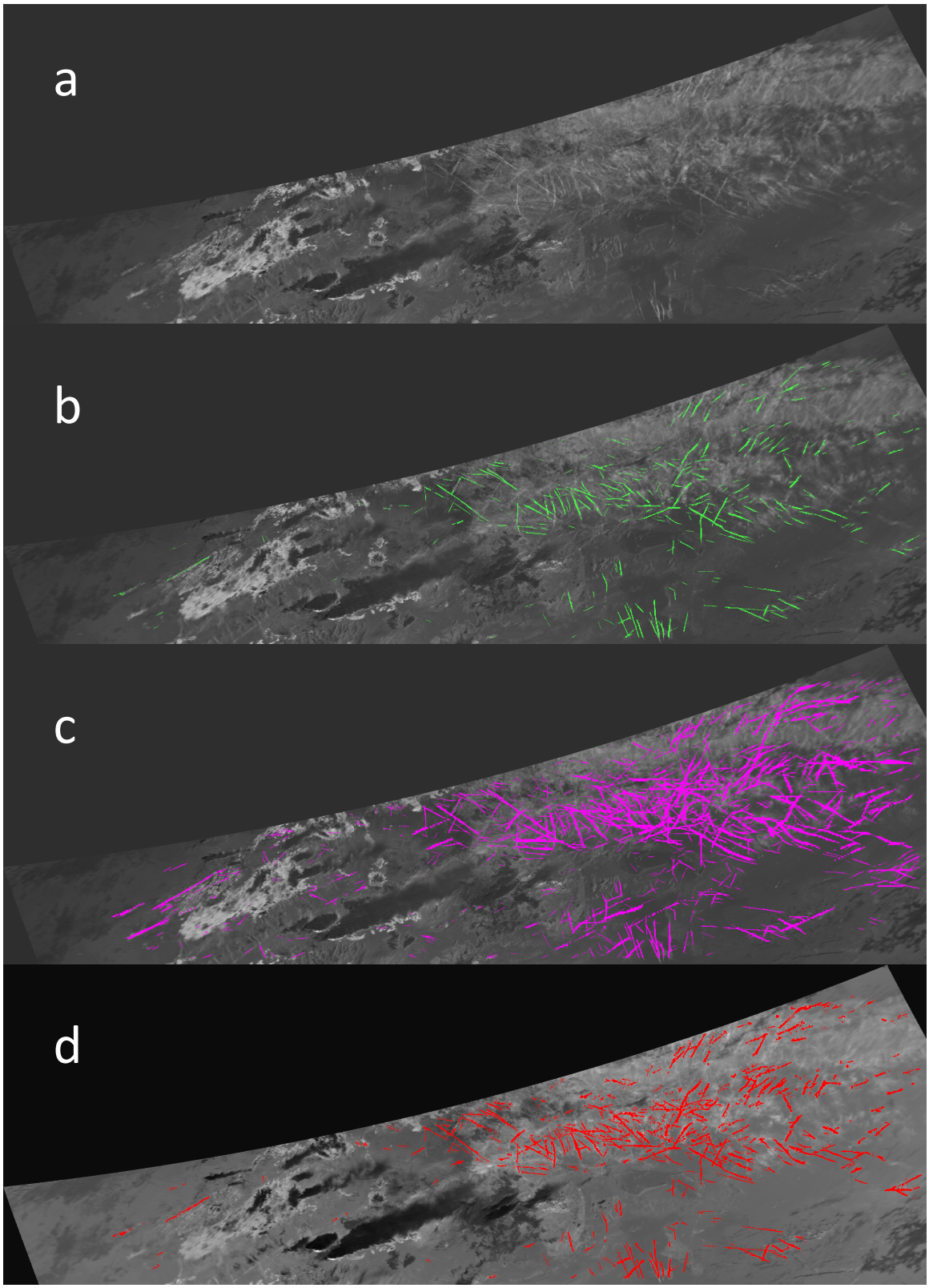

Figure 6: (a) *Aqua* MODIS 11 minus 12 μm brightness temperature difference image from 1 Jan 2006 at 1840 UTC. (b) Contrail mask derived from CDA3 shown in green. (c) Contrail mask derived from more sensitive version of CDA shown in magenta. (d) Contrail mask derived from CDA with contrail widening shown in red.

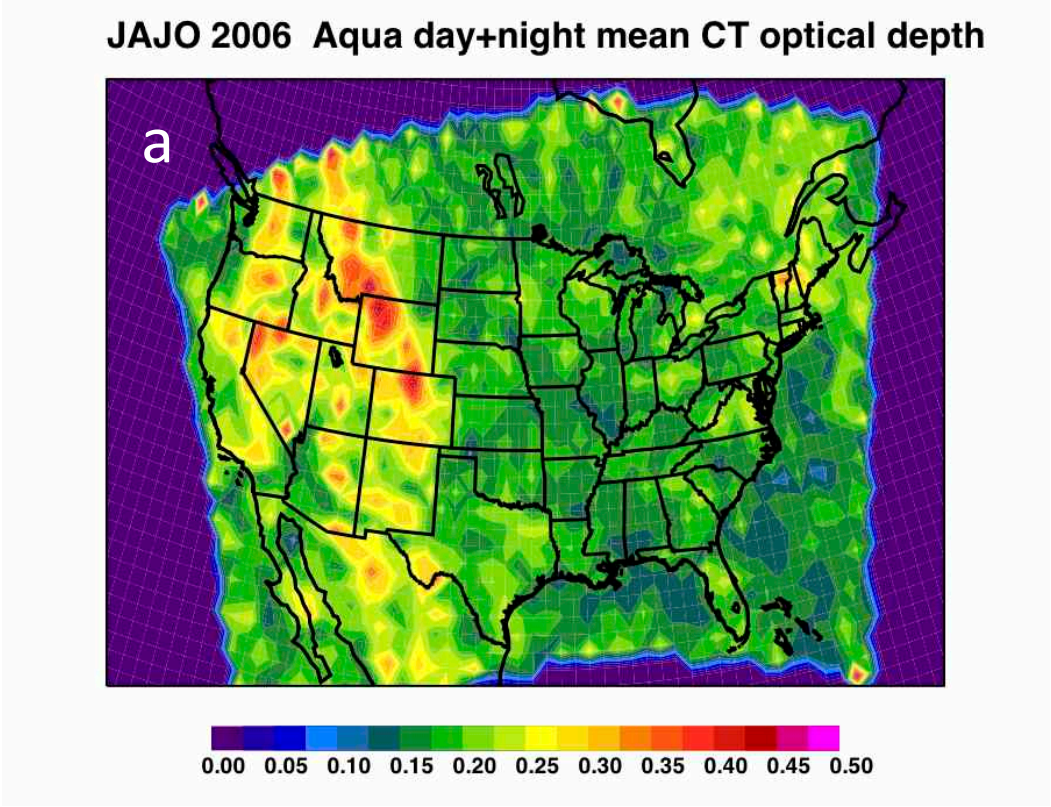

Figure 7: (a) JAJO 2006 mean day + night contrail optical depth computed from Terra MODIS over CONUS. (b) Same as (a), but computed over Europe.

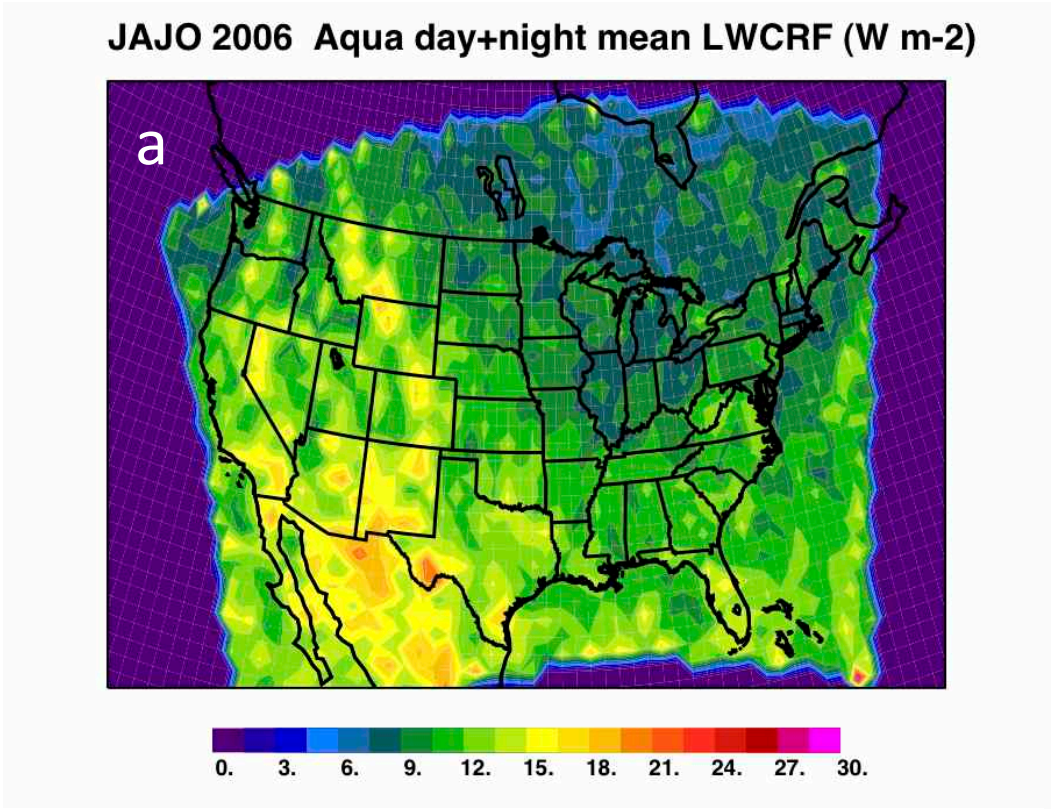

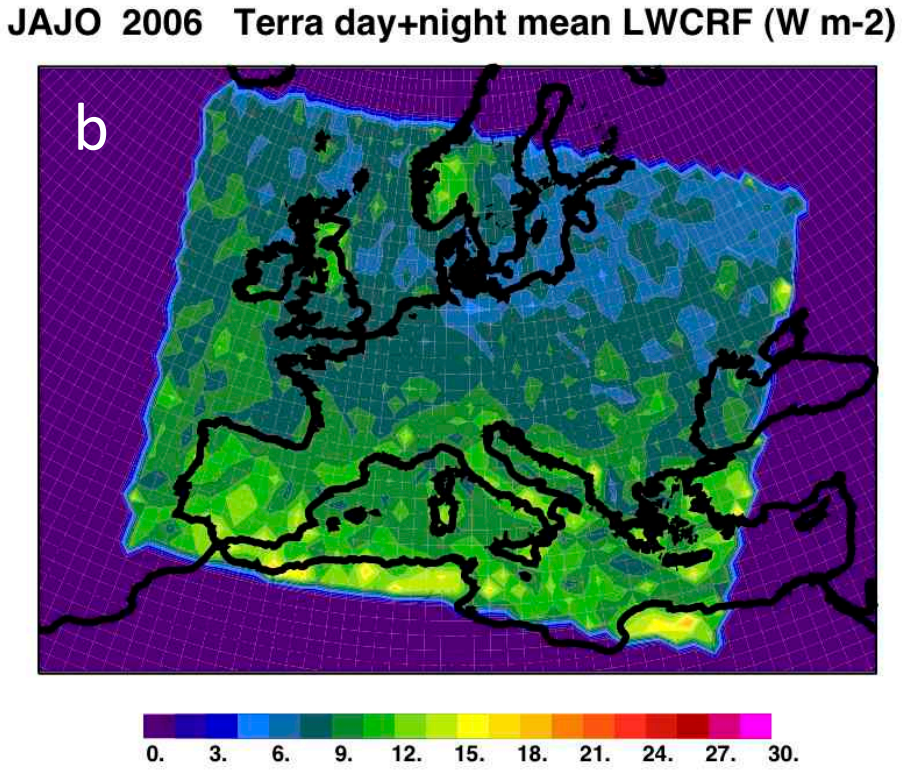

Figure 8: (a) JAJO 2006 mean day + night longwave radiative forcing in $W \cdot m^{-2}$ computed from Terra MODIS over CONUS. (b) Same as (a), but computed over Europe.